# WiMAX HAPS-Based Downlink Performance Employing Geometrical and Statistical Propagation-Channel Characteristics

**I.R. Palma-Lázgare**
**J.A. Delgado-Penín**

## Abstract

The evolution to a well-expected technology in wireless-communications maturity is in progress. Complementary applications are being suggested for such purposes, which might be possibly effective from the already ongoing research on high-altitude-platform systems. Herein, we introduce a HAPS-based system for delivering broadband communications intended to be operational at L band. A physical-statistical channel model for the HAPS-to-fixed-terrestrial terminal provision is derived from urban geometrical radio-coverage considerations with a simple diffraction theory. The stratospheric broadband channel model is fulfilled with the two channel-state situations related to the direct and specular rays, plus multipath. The first state consists of predicting the performance for which the line-of-sight path can exist between HAPS and the still terminal at street level. The second channel state refers to modeling the statistical fading characteristics for the shadowing condition. The system implementation is approximated and analyzed by performing intensive simulation-aided modeling. The proposed hypotheses use empirical data derived from land-mobile-satellite communication-system records. Because the systems require robust, reliable, and future standardization results, IEEE 802.16™-2004 PHY-layer technical specifications are used to accomplish the WiMAX HAPS-based downlink performance evaluation.

## 1. Introduction

A high-altitude-platform station (HAPS) is a stand-alone airship (or an airplane) stationed in the stratosphere at about 17-25 km above the Earth's surface. The expectation is to offer an alternative or complement to terrestrial and satellite-based communication systems. HAPS is also expected to make the most advantage of aforementioned technologies. It is presumed to have the capability of carrying a large variety of wireless-communications payloads [1-4]. A viable and futuristic framework for the HAPS telecommunications network architecture is displayed in Figure 1.

Satellite systems possess many attractive features, which are moderated by their disadvantages of large propagation delays (MEO and GEO satellite cases), and the unreliability of the satellite channel. Furthermore, the LEO satellite system has a high complexity. To this end, HAPs can be employed since they represent a solution preserving most of the advantages of satellites, while avoiding some of their drawbacks [5]. Looking at the terrestrial components, it is difficult and economically inefficient to cover remote and impenetrable areas with terrestrial wireless, wired, or fiber networks. However, HAPs constitute a real asset to wireless-infrastructure operators for providing telecommunication services over such areas [5]. In addition, two other applications of the HAP in the end-to-end path can be identified [5]: HAPs can be employed in isolation from any core networks to connect private networks (such as corporate LANs), or to provide trunk connections between core networks.

We now focus on the system's performance evaluation. For this, we intended to model the signal-processing actions with a more real, reliable, and robust approach. We described the signal-processing operations through a block diagram comprising the transmitter, the channel, and the receiver. As we focused on the impairments of the signal rather

*Israel R. Palma-Lázgare and José A. Delgado-Penín are with the Universitat Politècnica de Catalunya (UPC), Signal Theory and Communications Department, Campus Nord, C/Jordi Girona 1-3, Building D4, 08034 Barcelona, Spain; Tel: +34 934017214; Fax: +34 934017200; E-mail: ipalma@tsc.upc.edu; Tel: +34 934016815; Fax: +34 934016815; E-mail: delpen@tsc.upc.edu.*

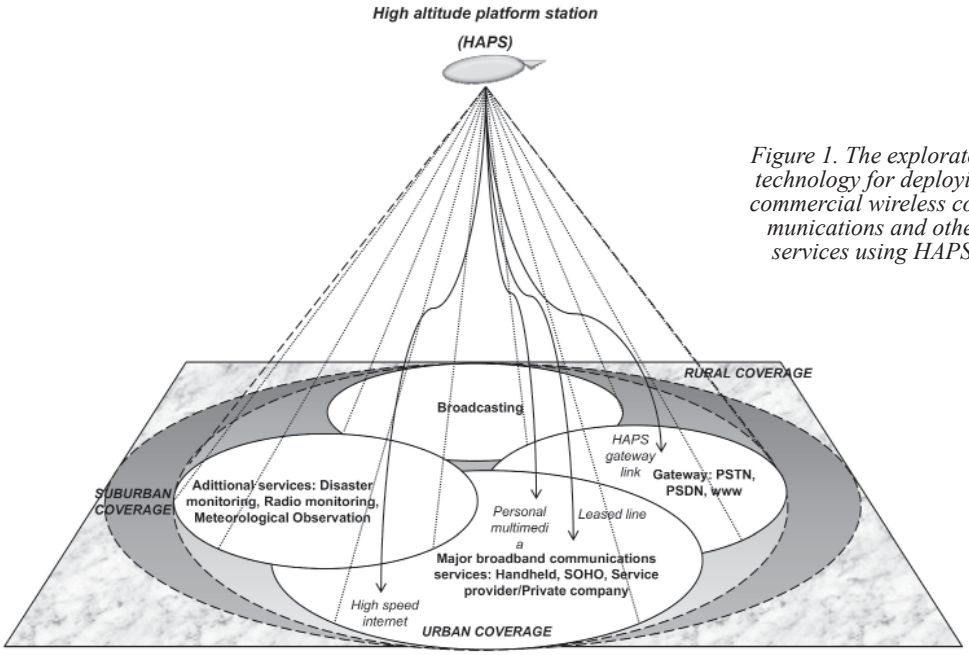


*Figure 1. The exploratory technology for deploying commercial wireless communications and other services using HAPS.*

than those from processing in the transceiver, the channel modeling was held as the main focus of our simulation work. The distinction we could derive here is that such signal processing was not highly precise, but it was worthwhile for the performance-evaluation and regulation issues.

We introduced the HAPS analysis with the proposal of modeling the stratospheric channel that would possibly be appropriate for a HAPS communications-link approach. For this, we required a controlled environment, in which suitable equipment and techniques may be implemented or be planned for testing. We have therefore considered the design approach referring to the propagation effects, with dependence on such a surrounding area for an end-to-end communication link. Although there are two existing impairment classes for the channel modeling, we have herein concentrated only on a specific class. In our case, the impairment class we refer to belongs to the channel and service environment that includes propagation effects of noise, fading, and shadowing. Atmospheric effects were neither considered from the stratospheric altitude nor for the considered operating frequency band. The remaining second class of impairments (i.e., phase noise and offset, channel nonlinearities, adjacent/co-channel interference, and HAPS/terminal motion) was not considered in our analysis, being considered for future analytical approaches.

Even though there are a lot of references for wireless-channel characterization dedicated to conventional terrestrial and satellite links, specific conditions in the stratospheric outdoor geometry require further investigation for the particular HAP-based system application. We state that there are a couple of radio-link types between the HAPS payload and the ground equipment: the gateway and the service link. For our case, we focused on the service link, where communications can occur between HAPS and the terrestrial still terminal in a cellular configuration mode.

The terrestrial terminals were described as being inside the urban zone, or urban area coverage (UAC) [6]. In this, we put into practice an important method of having urban coverage to the receiver antenna above, on, or below roof level. This work dealt specifically with the examination of a communication-link approach, with the physical characteristics presented in terms of the unobstructed or built-up conditions at a specific elevation angle, $\alpha$ , in which land-mobile satellite system (LMSS) research deployment and measurements were adopted to our HAPS proposal. The rationale behind such a proposed selection was remarked on in [7-8]. Propagation for HAPS communications behaves practically in the same manner as for the land-mobile satellite system case where similar elevation angles can be used. However, a difference is the link length, which sets the free-space loss reference level. It is also very distinctive that the land-mobile satellite system or HAPS channel was compared to the model where only a single distribution (or one single channel state) can no longer describe its behavior. HAPS and satellite communications were determined by more than two conditions of the radio link (e.g., the link being available when there was line of sight, or otherwise being in the unavailable shadowing/blockage case). Accordingly, we have also come to terms for the HAPS/satellite in which the channel model can be chiefly characterized by the geometry statistics of the terrestrial terminal environment.

We now emphasize the advantage and application for the two considered statistical and site-specific model categories. The assumed physical environment is open to reflection, scattering, and diffraction, thus path loss via base ray tracing was conceived. The case of the ray-tracing application resulted from the strategy to offer a path-loss formulation by assuming a finite number of reflectors. A reflector was considered as another source of signal, and the resultant signal at the receiver was the sum of signals

coming from all such sources with different distances and altered antenna fields. On the other hand, statistical/empirical modeling was carried out to provide an accurate formulation demanded by complex broadband communications, as well as to give an approach to low-computational-cost but robust channel modeling under urban conditions with appropriate records from the field.

Moreover, it seems that HAPS systems will operate in bands below 10 GHz, where shadowing/blockage plus multipath effects are dominant. Systems operating in these bands will most probably be based on a multi-carrier physical layer, such as that proposed in the WiMAX standard for the lower frequency bands. Hence, the pertinent HAPS-based system was evaluated under the adaptive parameters of the IEEE 802.16-2004 standard [9]. The frequency band of 1.820 GHz was used in our proposal to become the closest and a desirable approach to a representation of the 2 GHz band, over which the ITU has allocated the application of FBWA and next-generation mobile communications [6] based on a stratospheric platform using IMT-2000/IMT-Advanced technologies [10]. The thinking is to employ HAPS to supply flexible high-speed last-mile WiMAX provisions, with a rapid-deployment cost-effective wireless solution. It is also to have the HAPS application provide higher quality than satellite communications, with a lower propagation delay/distance and a more extensive area to cover than the terrestrial wireless system, the radio link of which is mostly blocked by terrestrial structures and vegetation.

Finally, the overall examined system performance was evaluated in terms of the average bit-error rate (BER), based on the proposed stratospheric-channel model and HAPS scenario. The system approach was based on computer-aided predictions (using *MATLAB*® software).

## 2. HAPS-Based System Scenario and Precursory Specifications

We looked at the global system geometry before its evaluation, so that the differences with respect to other radio systems could be clearly established [5, 11]. The global geometry can be represented as in Figure 2 for the HAPS-based system. This involves the Earth's curvature; a fixed position at an altitude $r_{HAPS}$ over the point *C*; and a direct path illuminating the fixed ground terminal with an elevation angle $\alpha_{Earth}$. Point *O* represents the Earth's center, and $r_{Earth}$ is the Earth's radius. The following expression follows from the principles of trigonometry:

$$\frac{\overline{OA}}{\sin\beta_{Earth}} = \frac{\overline{OB}}{\sin(90+\alpha_{Earth})} = \frac{\overline{OB}}{\cos\alpha_{Earth}}, \quad (1)$$

so
$$\sin\beta_{Earth} = \frac{r_{Earth}}{r_{Earth}+r_{HAPS}}\cos\alpha_{Earth}. \quad (2)$$

Assuming that the Earth's surface has a perfect spherical shape, the arc *AC* indicates the radius of the coverage from the HAP on the ground, expressed by the following equation:

$$\widehat{AC} = \gamma_{Earth} r_{Earth}; \quad (3)$$

Let us consider the triangle *OAB*. The total internal angle of the triangle is 180°, so the angle $\gamma_{Earth}$ satisfies the equation

$$\gamma_{Earth} = 90° - \alpha_{Earth} - \beta_{Earth}. \quad (4)$$

After substitutions, we are able to rewrite the radius of the HAPS' area coverage as follows:

$$R_{HAPS} = r_{Earth}\left[\cos^{-1}\left(\frac{r_{Earth}}{r_{Earth}+r_{HAPS}}\cos\alpha_{Earth}\right) - \alpha_{Earth}\right]. \quad (5)$$

$r_{Earth} = \frac{4}{3}6378$ km was used, instead of only the effective Earth's radius of 6378 km. This was done to consider atmospheric refraction that causes bending of the radio wave's path, and to compensate for the geometry at the time of linear propagation.

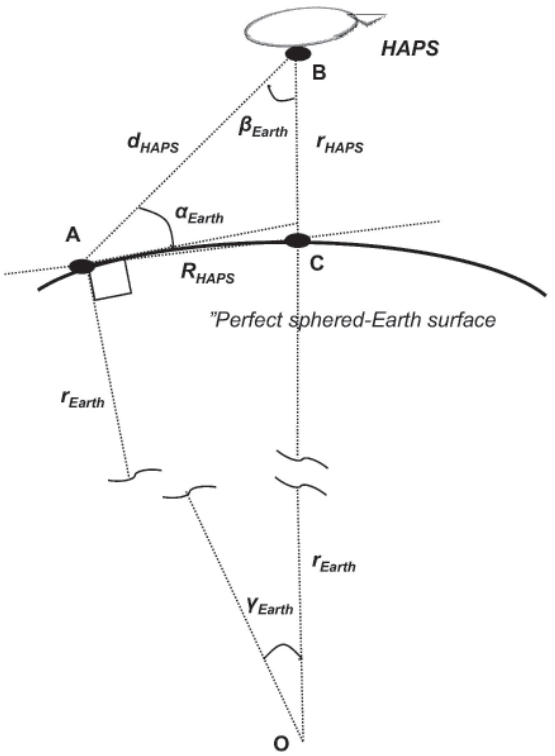


*Figure 2. An early geometry of the HAPS-based proposal (not to scale) [6, 13, 14].*

Regarding the above geometrical analysis, a HAPS at an altitude of 21 km has the capability of covering an area on the ground up to 419.6 km in diameter for 5° of elevation angle.

## 3. Performance Prediction

### 3.1 Preliminaries

An adequate HAPS-based radio-propagation channel model was developed. The geometry approach in Figures 1-4 was presumed, with elemental rays (or echoes) for the purpose of defining the channel conditions. At this stage, the stratospheric propagation link was established so as not to introduce other atmospheric mitigating factors, such as atmospheric refraction, precipitation (rain, fog, snow), cloud cover, and to not result in additional loss of the signal.

Two radio-propagation channel conditions were defined for the specific urban-area coverage. The first condition belongs to the line-of-sight situation, and the second belongs to the log-normal shadowing situation. For both situations, we needed to seize the pertinent propagation parameters for the "stratospheric habitat," considering the signal attenuation as a random process due to fast and slow fading variations arising from the channel's condition.

The extrapolation effort for the satellite-to-HAPS-based system scenario was assumed for the complex urban scenario, and to connect in appropriate fashion to the HAPS-to-ground design and solution. "Multi-mode channel-state modeling" in our case does not stand for the representation of the channel transitions between states (or non-stationary process). We assessed two proper single statistical processes that reviewed two independent stationary single-mode channel-state models occurring in the metropolitan scenario. For these, the state-oriented channel modeling was based on empirical land-mobile satellite system models to produce the approach to HAPS behavior. No possible extensions to an adaptable mobile scenario were used, due to the need for extensive HAPS communication measurement campaigns, or some extended approach from the satellite-based systems (e.g., by using the already proposed scheme of a multi-state chain process), referring us to mobility from the ground terminal and the platform, as well.

The HAPS-based system can have a higher line-of-sight probability because of the considerations of being an ultra-high-altitude tower, compared with a terrestrial tower. As a result, HAPS can easily provide line-of-sight communication at high $\alpha$, where the links are relatively free of the influence of obstacles. Generally, the probabilities of having a line-of-sight path can be described by larger values of $\alpha$ ($> 40°$), and a shadowing path by lower values of $\alpha$ ($\leq 40°$), which would result in a high probability of the shadowing state. Nevertheless, when HAPS is used to serve an urban environmental area, buildings can stand – or even there could be skyscraper – where the condition of a line-of-sight path would be very difficult to have. In our case, since we have a heavily built-up area coverage, the shadowed region seemed large and was the most-severe attenuation factor. Shadowing-power attenuation was thus considered as another attenuation factor, in addition to the attenuation due to path loss. We remark that if a hillock appears in the radio-communication path, shadowing will be avoided and diffraction will instead appear.

Moreover, the determined signal transmission between HAPS and the ground terminal generally takes place via many paths, and the variation of $\alpha$ can define this. This last categorization might include one direct ray and the potential remaining multipath rays: line of sight, a single reflection from a building, a single reflection from the street, a double reflection from the building to the street, a double reflection from building to building, diffraction from the rooftop of a building, diffraction from a rooftop and a single reflection from a building, diffraction from a rooftop and a single reflection from the street, and diffraction from a rooftop and a double reflection from a building to the street. Rays outside the mentioned categories can be assumed to leave the original target. Since all surfaces in real propagation environments are finite, edges and corners also have to be considered. In our case, the situation called diffraction can occur when a large body obstructs the radio path between the transmitter and the receiver, causing secondary waves to be formed behind the obstructing body that continue to propagate towards the receiver.

The relevant model, with specific details of the building allocation, trees, etc., for the metropolitan environment, gives the signal-information approach. This sorts out an explicit ray-tracing solution for the electromagnetic wave's status that does not require a great deal of measurement data. It is a relatively generic channel model, which can be used for simulations.

The implementation of the ray-tracing algorithm in our system with relative large *d* corresponded to the two-ray model. As the stationary receiver was considered to be a gadget, station, or some small hardware for easy setup/deployment, and equipped with a low-gain antenna, the arrival rays collected by the terrestrial antenna included two coherent components. These were a direct path (a significant portion of the total energy arrives at the receiver by way of a direct wave), and a specular reflected path (the remaining power of the transmitted signal) – plus the diffuse components (many randomly scattered rays) [15]. In further detail, the frequently reflected path from the ground in satellite-based communications design was not proper in our HAPS-based communications interpretation. This was in a little contrast to the conventional non-mobile HAPS-to-ground link, carrying equipment including high-gain antennas at the receiver, which could completely reject both specular and diffuse components and collect only the direct path. The contribution of the wave reflected from building structures was considered, as well as possibly from trees nearby the receiver. Echoes that properly intersect

with the receiver were next analyzed. The power-delay profile (PDP) estimation was developed by mapping the power of the different rays with respect to the delay-time information [16, 17]. The diffuse components were considered to arrive at an elevation angle near 0° with uniformly distributed phase, with amplitude statistically described by a Rayleigh distribution, and a maximum Doppler spectrum of $2v_T/\lambda$ (denoting the small existing motion and the carrier wavelength, respectively). Thus, the approach of the aforementioned method considered the set of rays originating from the same source and reflected from the same set of surfaces to be part of the same wavefront.

We refer now to the connection of our proposed model to those with the closest relationship: the so-called (geometrical) single-bounce model, or other similar research (e.g., a circular straight cone geometry, or a three-dimensional ellipsoid propagation model). We refer specifically to distinctions for the specular reflection echo (single-bounce path) and the corresponding delay spread. We differed from those already established models by approaching the probability of the specular-ray's existence by means of the building blockage inside the impaired scatterer topography, resulting in a nonuniform coverage over the receiver. That is, we considered that the specular reflection ray came from a near scatterer with irregular environment volume, and not uniformly distributed in space to the receiver. We can add that the scattering loss that depended on the material of the structures was not totally clarified. Hence, power delay or other related angle calculations for the arrival rays were expressed differently from ours, because of different assumptions.

Eventually, we can remember that the product of the antenna fields for the corresponding peers is important in determining the received power. In the receiver's antenna, following the induction of electric currents created by the wave's arrival, the energy in our operating frequency band was directly coupled to antenna size. Equally, antenna size was directly coupled to the field's wavelength ( $\lambda$ ), which was basically inversely proportional to the carrier frequency ( $\lambda = c/f_c$ ). In other words, the higher the frequency, the smaller the antenna size. Hence, the antenna characteristics [11, 18] used during the analysis could have played an important role in affecting the performance outcome. Nevertheless, idealist for antennae comes for our whole analysis. Since we considered idealisms for the antenna onboard the platform, we used an ideal antenna pattern adopted for the HAPS application (denoted by the possible use of smart antennae or antenna arrays) and with a zero-dBi-gain omnidirectional antenna at the receiver terminal. Local mean received power (the local mean of the signals received) was thus directly dependent on $\alpha$ and on the transmitted power. Using a presumed omnidirectional antenna had the relevant aspect for our design of having the multipath power contribution be much higher than the use of a directional antenna.

## 3.2 Stratospheric Propagation Premises

The overall representation for the HAPS-channel modeling has been taken as the equivalent complex channel impulse response (CIR) expression [19]:

$$\tilde{c}(\tau,t) = \sqrt{Lf_{CS}(t)}\tilde{h}(\tau,t), \qquad (6)$$

where the first factor represents the long-term situation, and the second factor accounts for the short-term situation. Equation (6) is valid for values greater than 1 km, where $L$ is the mean loss, and $f_{CS}(t)$ belongs to the channel-state situation. For example, for the shadowing state (in the locality of the receiver) through time $t$, the function can be modeled as a Gaussian variable with 0 dB mean and a standard deviation (the log-normal model).

In order to model the single HAPS-to-terminal channel propagation for optimization, our design was comprised of two cascaded stages (see Figure 3a). These were associated with the HAPS-to-ground path (HAP process) and with the effects surrounding the terrestrial terminal that are relative to its neighboring scatterers (terrestrial process):

$$PL = PL_{HAPS} + PL_{Terrestrial}, \qquad (7)$$

For this – and considering similarities to land-mobile satellite systems – free-space attenuation and multipath fading effects counted for the major fading factors for our proposal.

From the entire model available for propagation-loss predictions – either for terrestrial or satellite-based applications – in our case, for the HAPS-based system, a general theoretical equation can be given as

$$PL_{total} = PL_{FSPL} + PL_{shadowing} + PL_{fading}, \qquad (8)$$

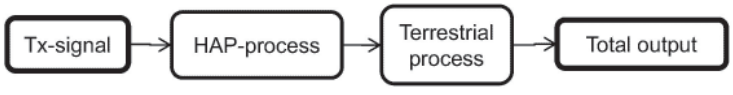


*Figure 3a. A representation of stratospheric channel modeling proposal.*

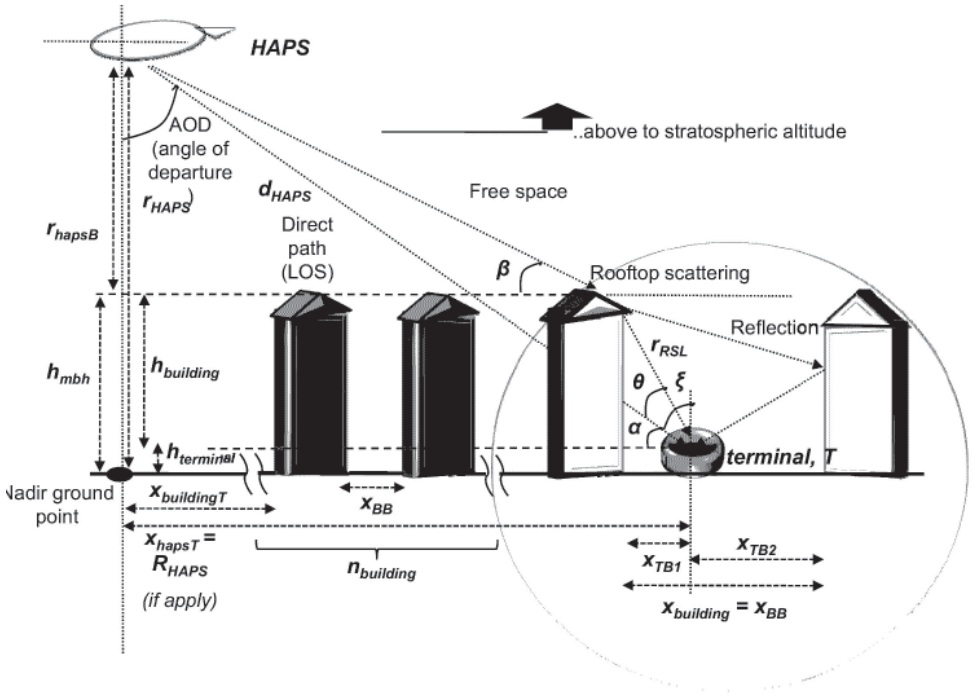


*Figure 3b. An idealized urban built-up geometry for the radio-propagation model for downlink HAPS-based communications (not to scale).*

where $PL_{total}$ is the total propagation loss, $PL_{FSPL}$ represents the free-space path loss as a function of the transmitter-receiver separation distance, $PL_{shadowing}$ denotes the shadowing loss, and $PL_{fading}$ is the local fading loss.

HAPS has been considered to be an extremely tall base station that can present a propagation path consisting of the free-space loss, diffraction from a rooftop, and multiple reflections from nearby buildings. Thereafter, based on Equation (7) and the theoretical propagation loss, the HAPS-based communications path loss can be represented as the sum of the free-space loss (FSL), the rooftop scattering loss (RSL), and the multiple-screen diffraction loss (MSDL). We thus supposed the total propagation loss to be power-summed, since it was desired to predict the local median value. The received power can be obtained from

$$PL = PL_{HAPS,FSL} + PL_{Terrestrial,RSL} + PL_{Terrestrial,MSDL} \quad (9)$$

The formulation for the free-space path loss is dedicated to the line-of-sight (LOS) case in which there is only one direct path from transmitter to receiver. The free-space path loss depends only on the frequency and the separation distance between transceivers, as typically expressed by the fixed quantity

$$PL_{HAPS,FSL} = 10\log_{10}\left(\frac{\lambda}{4\pi \cdot d_{HAPS}}\right)^2 \text{ [dB]}, \quad (10)$$

where $\lambda$ is the wavelength in meters, and $d$ represents the transmitter-receiver distance. The free-space loss equation is only a valid predictor for values of $d_{HAPS}$ that are in the far field of the transmitting antenna:

$$d_{HAPS} = \sqrt{R_{HAPS}^2 + r_{HAPS}^2} \,. \quad (11)$$

Now, the diffraction from the rooftop down to the street level (as shown in Figure 3b) leads to an excess loss at the ground terminal, *T*, expressed by

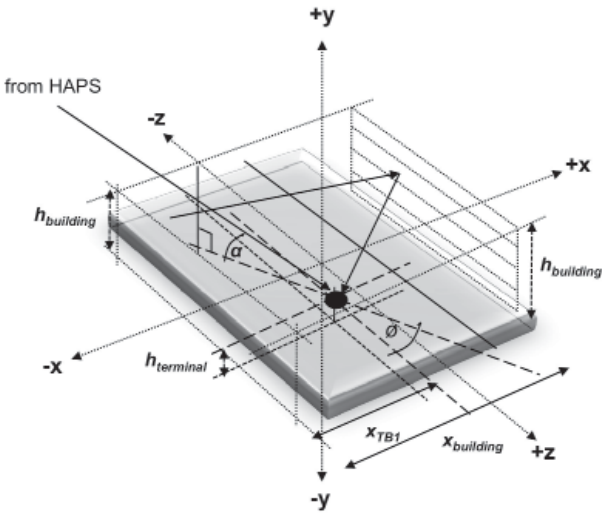


*Figure 3c. The geometry for the radio propagation model at street level.*

$$PL_{Terrestrial,RSL}$$

$$= \min\left\{10\log_{10}\left[\frac{\lambda}{2\pi^2 r_{RSL}}\left(\frac{1}{2\pi\theta}\right)^2\right], PL_{EPLMRB}\right\}, \quad (12)$$

where $PL_{EPLMRB}$ is the excess propagation loss due to multiple reflections from the buildings' walls along the street and surrounding *T*. From Equation (12) and Figure (3c), it can be shown that

$$\theta = \left|\tan^{-1}\frac{h_{building}}{x1} - \alpha\right|,$$

$$r_{RSL} = \sqrt{h_{building}^2 + x_{TB1}^2}, \quad (13)$$

$$x1 = x_{TB1},\ h_{building}\cot\alpha \le x_{TB1},$$

$$x1 = 0,\ h_{building}\cot\alpha > x_{TB1},$$

where $h_{building}$ is the difference between the height of the building and the terrestrial terminal's height, $x_{TB1}$ is the horizontal distance between the terminal and the diffraction edge (shadow), and $x_{BB}$ is the width between the supposed buildings at both sides of the street.

For this scenario, $x_{TB1}$ is given by

$$x_{TB1} = \min\left\{\frac{x_{BB}}{2}, h_{building}\cot\alpha\right\}, \quad (14)$$

with the second term, $h_{building}\cot\alpha$ being the width of the building's shadow cast onto the street level. When $\alpha$ is close to 90º, shadowing is narrow, and the rooftop diffraction loss is relatively small. In the case of a smaller $\alpha$, the rooftop diffraction loss might be very high, and the user terminal would receive multiple reflection signals from the sides of nearby buildings. The condition for multiple side reflections is satisfied if

$$x_{BB} \le h_{building}\cot\alpha. \quad (15)$$

The number of reflections, $N_{RB}$, caused by when rooftop diffraction has occurred (from the opposite building on the other side of street) can be estimated by

$$N_{RB} = \text{int}\left(\frac{h_{building}}{x_{BB}\cot\alpha} - 1\right), \quad (16)$$

where the function $\text{int}(\ )$ means the largest integer that is smaller than or equal to the variable inside. The excess propagation loss due to reflection can thus be computed if the incident angle and the real and imaginary parts of the dielectric constant of the building material are known. However, except for "grazing" reflection, where the signal essentially propagates parallel to the building's surface, the excess loss can be taken to be $\sim 10$ dB. The multiple reflection loss is

$$PL_{EPLMRB} = -10N_{RB}. \quad (17)$$

Subsequently, we can speculate that the rooftop diffraction loss can be typically of the order of 10 to 40 dB, meaning that more power is needed for communications between a terminal and HAPS in the shady area. In addition to this, it is also possible to assume that at most two reflections must take place before the signal can reach the terminal (one of them must be a reflection from the ground, which is disregarded in our model). Let us take a reference from an example of a typical urban built-up situation. Both the street width and the building height are of the order of 25 m or greater. Accordingly, $N_{RB}$ does not exceed two until $\alpha$ is below 19°, i.e., in an urban or suburban area with low building (building heights lower than 10 m and street widths of around 35 m), $\alpha$ would be less than 5.5º before $N_{RB}$ becomes greater than two. Consequently, at different greater $\alpha$ values and coverage areas, the excess loss should be of the order of 20 dB or less. Moreover, we can mention that in the region of typical residential areas, outdoor radio propagation is dominated by line-of-sight propagation and rooftop diffraction. The absence of multiple reflections means that the terminal on the shady side will have to rely on rooftop diffraction to provide coverage, and it is very significant that multiple reflections could be rarely effective because of the inter-built-up distances.

Moving to the next parameter, multiple-screen diffraction loss – which differs from the multiple-screen diffraction loss of the traditional radio tower ground base station – we assumed that the data link transmission passes a row of buildings until reaching the last structure next to the terrestrial terminal. Multiple-screen diffraction loss can thus take the following general form:

$$PL_{Terrestrial,MSDL} = 10\log_{10}\left(Q^2\right), \quad (18)$$

In the HAPS case, the factor *Q* depends on $\alpha$ relative to the location of the terminal. For most elevation angles, $PL_{Terrestrial,MSDL}$ is essentially zero. At very small $\alpha$, $PL_{Terrestrial,MSDL}$ increases rapidly. At zero elevation angle, $PL_{Terrestrial,MSDL}$ becomes arbitrarily large, so that only line-of-sight propagation is practically possible. We can examine and apply the case of multiple-screen diffraction for $\alpha$ with values greater than 3º. From the consideration of diffraction fringes between two successive screens, we are led to the following dimensionless variable:

$$\chi = \tan\alpha\sqrt{\frac{x_{BB}\cos\alpha}{\lambda}}\,, \qquad (19)$$

which corresponds roughly to $\chi$ being greater than one (for typical average building separations of about 50 m), and the multiple-screen diffraction loss becomes effectively zero. For this reason and because of the long coverage distance from HAPS, multiple-screen diffraction is not a significant loss factor in the main HAPS service area (we would say at values around and greater than 45º).

After these last definitions, in our case, the feasible total transmission loss becomes

$$PL\,|_{shadowing} = 10\log_{10}\left[\left(\frac{\lambda}{4\pi d_{HAPS}}\right)^2\right]$$

$$+\min\left\{10\log_{10}\left(\frac{\lambda}{2\pi^2 r_{RSL}}\left[\frac{1}{2\pi\theta}\right]^2\right),\right.$$

$$\left.10\,\mathrm{int}\left(\frac{h_{building}}{x_{BB}\tan\alpha}-1\right)\right\}, \qquad (20)$$

$$PL\,|_{LOS} = 10\log_{10}\left[\left(\frac{\lambda}{4\pi d_{HAPS}}\right)^2\right].$$

Further, we obtained further improvements in our system, covering the topic of prediction models of radio wave propagation in built-up areas, to explicitly take into account building diffraction effects to improve accuracy. At this point, we recapitulate some terminology.

The presumed built-up model has been found useful for a real-case approach where the positions of individual buildings were certainly unknown, but where some estimates of the mean building height and spacing were available. The allocation of the buildings on the ground, between the HAPS-nadir point and the receiver, were of approximately uniform height and spacing, even if there were a large number of them. It was assumed that the average building height was 20 m, having an approximation to the Rayleigh distribution. This resulted in a situation where the probability of the line-of-sight state would go down if the average building height increased. The inter-building street width was assumed to be equal to or slightly wider than a real average street width, and a constant mean inter-building spacing, $x_{building}$ (or $x_{BB}$) was assumed. Referring to the receiver, it was located in a position where it was surrounded by buildings on the right and left sides along the street. The receiver was assumed to be least 1 m in height. It could be located at some point across the width of the street, and not necessarily in the middle of the two surrounding buildings.

A solution for diffraction modeling purposes was therefore obtained. Buildings were conventionally viewed as parallel absorbing half planes (knife edges), located at the peak of the building's rooftop [20] (see Figure 3b). The attenuation function was provided from the complete solution to the problem of multiple collinear knife-edge diffraction with an arbitrary number of edges. The solution focused on the particular resolution for the multiple-edge diffraction integral from Vogler's model, utilizing a method of repeated approximation for the resulting integral equation [20]. The terrestrial antenna was placed at an arbitrary height, and located some distance away from the row-building's edges. The field was computed at a reference point located at the rooftop of the final building. The field strength at street level was then calculated by a simple single-plane approximation for each of the rays arriving at the receiver. The solution was uniformly valid, so that the source point could be above, level with, or below the diffraction-edge height. It was equally possible to easily apply it to a small or large number of edges.

From the shadowing attenuation theory, a more complete received power approach can be calculated. The condition is now clearly defined for a single knife-edge diffraction attenuation at the rooftop of the closest building to the ground terminal. This model, proper in the line-of-sight and shady circumstances, allowed us to make predictions where direct measurements were unavailable, and where existing land-mobile satellite system records could be adopted [8, 20].

For the obstructed condition, we assumed the attenuation from the free-space field to be determined by the two practical diffracted and reflection diffracted rays (triggered by the building opposite to the main building), which were combined with random phase at the receiver:

$$PL_{Terrestrial,DS}$$

$$= PL_{HAPS,FSL}\sqrt{A^2(\vartheta_{DLOS}) + \rho^2 A^2(\vartheta_{DSR})}\,, \quad (21)$$

where $\rho$ is the loss because of reflection, including effects due to polarization, surface roughness, and the material's reflection coefficient. Furthermore,

$$A(\vartheta_{DLOS}) = \tfrac{1}{2}F(\vartheta_{DLOS})e^{-j\pi/4} + \tfrac{1}{2}\,, \qquad (22)$$

$$A(\vartheta_{DSR}) = \tfrac{1}{2}F(\vartheta_{DSR})e^{-j\pi/4} + \tfrac{1}{2}\,,$$

where $F$ is the complex Fresnel integral,

$$F(\vartheta_D) = C(\vartheta_D) + jS(\vartheta_D). \quad (23)$$

The Fresnel diffraction parameters for the diffracted ray and for the reflection diffracted ray are given by

$$\vartheta_{DLOS} = -\left[\frac{\pi}{2} - \tan^{-1}\left(\frac{x_{TB1}}{h_{building}}\right) - \alpha\right]\sqrt{\frac{2x_{TB1}}{\lambda}}, \quad (24)$$

$$\vartheta_{DSR} = -\left[\frac{\pi}{2} - \tan^{-1}\left(\frac{2x_{building} - x_{TB1}}{h_{building}}\right) - \alpha\right]$$

$$\sqrt{\frac{2\left(2x_{building} - x_{TB1}\right)}{\lambda}}.$$

In due course, for the line-of-sight condition, we power-summed the respective direct and specular reflection rays:

$$PL_{Terrestrial,DD} = P(\vartheta_{LOS}) + \rho^2 P(\vartheta_{SR}), \quad (25)$$

with the diffraction parameters defined for the direct, $\vartheta_{LOS}$, and reflected, $\vartheta_{SR}$, rays as

$$\vartheta_{LOS} = \left(h_{building} - h_{LOS}\right)\sqrt{\frac{2}{\lambda d_{LOS}}}, \quad (26)$$

$$\vartheta_{SR} = \left(h_{building} - h_{SR}\right)\sqrt{\frac{2}{\lambda d_{SR}}}, \quad (27)$$

where

$$h_{LOS} = \begin{cases} h_{terminal} + \dfrac{x_{TB1}\tan\alpha}{\sin\phi}; & 0 < \phi \le \pi \\ h_{terminal} + \dfrac{(x_{BB} - x_{TB1})\tan\alpha}{\sin\phi}; & -\pi < \phi \le 0 \end{cases},$$

$$d_{LOS} = \begin{cases} \dfrac{x_{TB1}}{\sin\phi\cos\alpha}; & 0 < \phi \le \pi \\ \dfrac{(x_{BB} - x_{TB1})}{\sin\phi\cos\alpha}; & -\pi < \phi \le 0 \end{cases}, \quad (28)$$

$$h_{SR} = \begin{cases} h_{terminal} + \dfrac{(2x_{BB} - x_{TB1})\tan\alpha}{\sin\phi}; & 0 < \phi \le \pi \\ h_{terminal} + \dfrac{(x_{BB} + x_{TB1})\tan\alpha}{\sin\phi}; & -\pi < \phi \le 0 \end{cases},$$

$$d_{SR} = \begin{cases} \dfrac{(2x_{BB} - x_{TB1})}{\sin\phi\cos\alpha}; & 0 < \phi \le \pi \\ \dfrac{(x_{BB} + x_{TB1})}{\sin\phi\cos\alpha}; & -\pi < \phi \le 0 \end{cases}.$$

The diffracted ray power was then expressed in terms of the Fresnel cosine, $C(\vartheta)$, and sine, $S(\vartheta)$, integrals:

$$P(\vartheta) = \tfrac{1}{2}\left[\tfrac{1}{2} + C^2(\vartheta) - C(\vartheta) + S^2(\vartheta) - S(\vartheta)\right]. \quad (29)$$

The latter expressions were assumed to have HAPS-to-building distances very much greater than the building-to-terminal distances. It was also supposed that only one building contributed to the diffraction process. This meant that the higher the building height was, the more it would count for the shadowing-case attenuation.

The typical extent of vegetation areas in cities is generally too small, but realistically it exists. A similar analysis was been applied to potential shadowing by trees rather than buildings, and the explanation is as follows.

In our case, the effect of foliage was considered by adding contributions from the penetration through vegetation (empirical approach), and diffraction over vegetation effects [35]. The foliage accounted for leaves very thin from real vegetation canopies behaving like Rayleigh scatterers, without considering the influence of the stem and moisture. The diffraction over the greenery was thus specifically modeled by a single knife-edge diffraction at 1.2 m average height. Penetration through the greenery was defined to be feasible with 5 dB, by the following approach:

$$PL_{Terrestrial,foliage} = g\sum_{i=1}^{n} l_i \text{ [db]}, \quad (30)$$

where $g = 0.2$ dB/m, and $l_i$ stands for the longitude of the $i$th vegetative area. This was taken as an alternate arrangement, with $n = 5$ greenery areas of 5 m in longitude for each one, and they were located through the signal transmission path.

## 3.3 Channel Characterization

All of these models could certainly be used to predict the narrowband characteristics. In order to acquire the right predictions for the signal for the broadband case – without requiring in-depth usage of site-specific information, and gaining time in the computation – a more promising approach of characterization of the delay spread and fading statistics must keep the system performance conjecture within a small margin error.

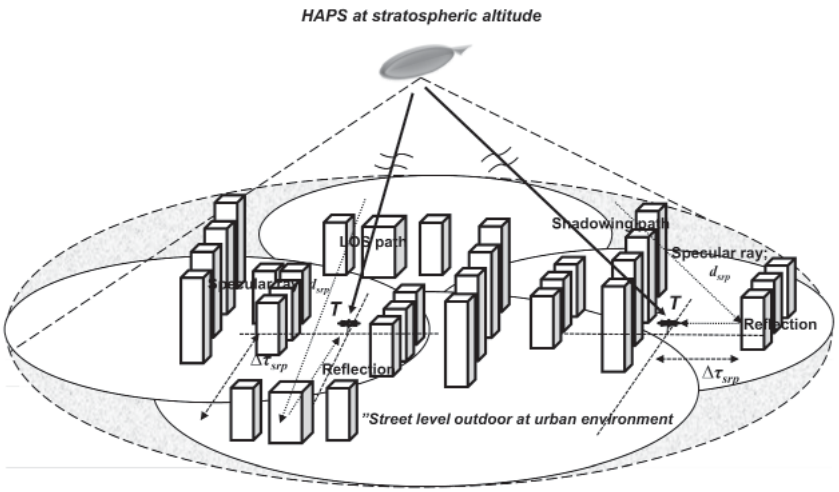


*Figure 4. Based on the HAPS channel conditions and the presence or absence of smooth and rough outdoor surfaces, profiles of direct and specular reflection paths plus multipath in the urban built-up area are manifested.*

In this proposal, a viable model was useful for developing the information regarding the broadband characteristics by means of the propagation prediction using the echo/ray terminology at local levels of *T* surroundings. Scattering occurred due to the radio wave infringing on a large rough surface (or on dense foliage) that caused the (reflected) rays to spread out in various directions, or due to the motion of objects nearly surrounding the terminal. The proposed propagation model was theoretically based on the geometrical features of the built-up structures surrounding the ground terminal. It was expanded with statistical estimation from the land-mobile satellite system channel model, in order to estimate the system's field capacity. The predictions were realized to be fairly different from those of the terrestrial channel, but rather similar to the satellite channel.

The evaluation of the downlink performance using the HAPS-communications channel necessarily requires a fading mitigation technique (i.e., in our analysis the use of coded orthogonal frequency-division multiplexing (COFDM) [23-24] was proposed, aiming a the standardization of the ITU administration under the IMT-2000 and IEEE frameworks) to ensure the channel quality being above a minimum level of performance. In our case, the performance evaluation was expressed in terms of the achievable bit-error rate (BER). The evaluation was able to carry broadband and other communications services at different information bit rates (allowing adaptability of the system to on-demand circumstances). It is important that we recall certain system characterizations from the research presented in [25, 26]. The channel modeling representation was treated with some similarities from these studies. The model was conformed to the hypotheses of a direct ray and a specular-reflection ray (a reflected signal caused by a "reflection body" inside the small vicinity of the receiver), plus multipath from two such main rays. These corresponded to and were added for the characterization of the already considered channel states of shadowing and unobstructed path, with a log-normal distribution [27] and a Rice distribution [28], respectively. The practical infrastructure is represented in Figures 4, 5, and 6.

Previously, we introduced that the ray components of the radio signal can establish the signal attenuation for a deterministic channel. In our case, the channel is time varying. Such statistical properties were analyzed with the Bello functions [29] as the base of our short-term-variation modeling. We reorganized the latter statistical characterization and simplified the channel to the WSSUS

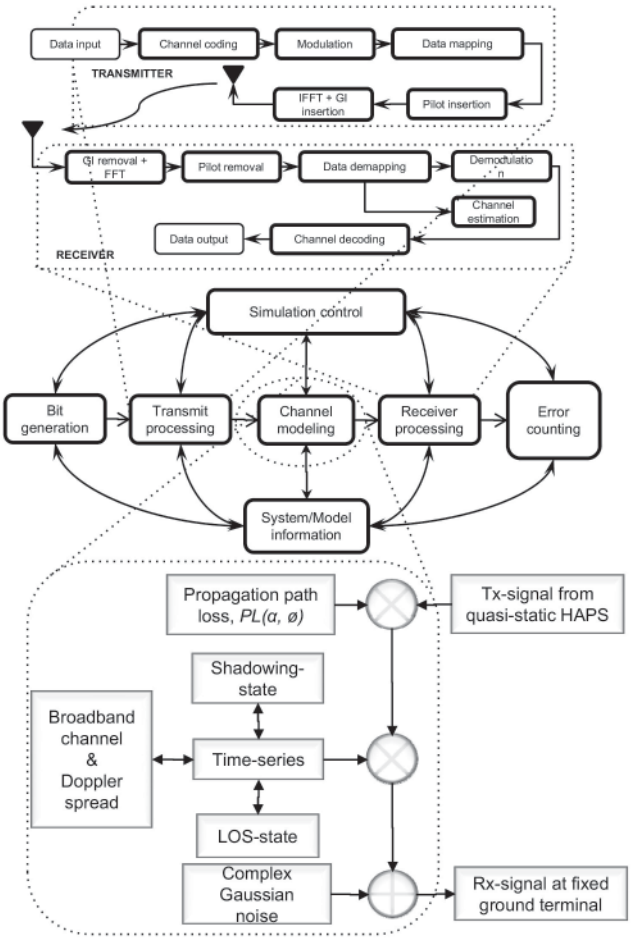


*Figure 5. The simulation control for the overall stratospheric broadband channel modeling pro-*

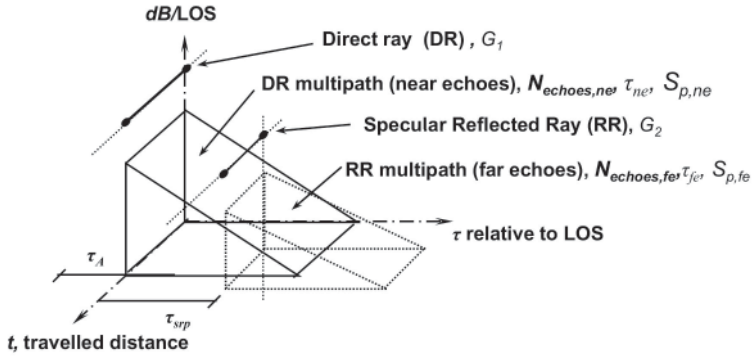


*Figure 6a. An illustrative representation of the broadband channel modeling simulator for the physical echoes and multipath fading [8, 25, 26].*

function, as shown in Figure 6, with a tapped-delay-line model of 11 bins.

In the last account, broadband characterization was not completely acquired, even using the characterization from [25, 26] and their references. Herein, our system exigencies claim further accurate signal predictions related to achieving a smaller margin of error.

Once we declared the major parameters and that the receiver had an elevation angle less than 45º, the significant parameter of the shadowing effect was taken to be a time sharing of shadowing of the order of 50%. Attending to this last topic, we can present one more analysis to be counted for performance in the shadowing channel condition in terms of visibility and building-height distribution.

Visibility was supposed to be the probability of the channel of having a line-of-sight situation at each elevation angle and within 360º of the azimuth angle $\phi$ (a variable referenced in Figure 3c). Thus, the equation for visibility was based closely on the significances of $\alpha$ and $\phi$ [13, 30]:

$$p_{vis}(\alpha,\phi) = \begin{cases} (\sin\alpha)^{0.01}; & \phi = 0^{\circ} \\ (\sin\alpha)^{\sin\phi}; & \phi = 30^{\circ}, 60^{\circ}, 90^{\circ} \end{cases}, \quad (31)$$

where $\phi$ was $\leq 10°$ for line of sight and $> 75°$ for shadowing. $\phi = 0°$ in the negative *z*-axis direction and $\phi = 90°$ in the negative *x*-axis direction, as shown in Figure 1. The visibility was respectively in agreement with the direct path at $\phi = 0°$ and the shadowing situation being an increasing function following high $\phi$. At this point, we can say that the propagation impairments for the line-of-sight situation went along with the variations in $\alpha$. In the obstructed situation, different values of $\phi$ resulted in different fading, because of the dominant multipath power variations, with worse effects at $\alpha < 45°$. The potentially worst case occurred when $\phi = 90°$, for which a distributed Rayleigh characterization was roughly an adequate approach.

We can state that the ray was also judged [20, 21] to be shadowed when the building height, $h_{mbh}$, exceeded some threshold height, $h_{threshold}$, relative to the point of the direct ray's height. The shadowing probability term, $P_{building}$, was expressed by the probability density function (PDF) of the building height, $p_{building}(h_{mbh})$:

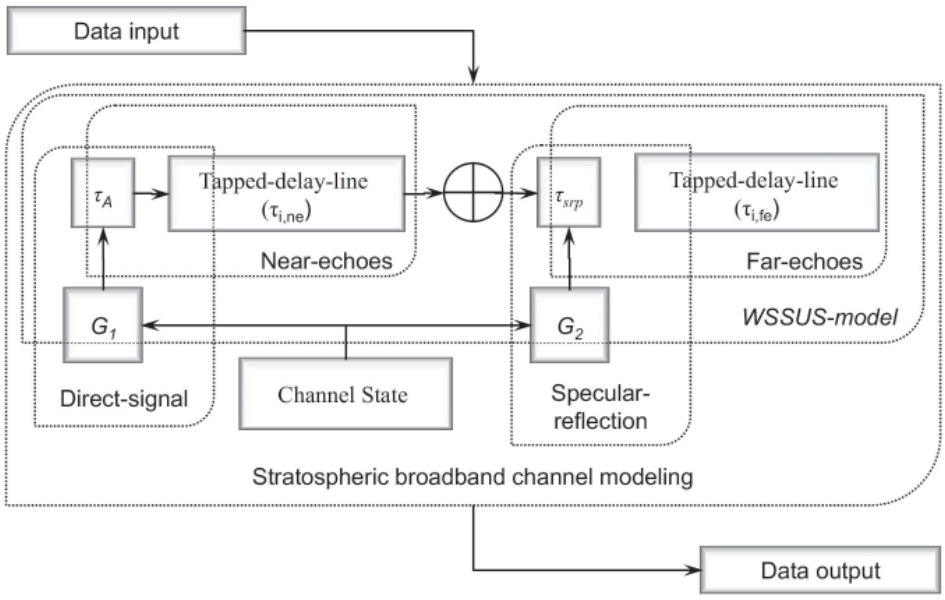


*Figure 6b. A channel-state diagram of the broadband channel modeling simulator for the physical echoes and multipath fading [8, 25, 26].*

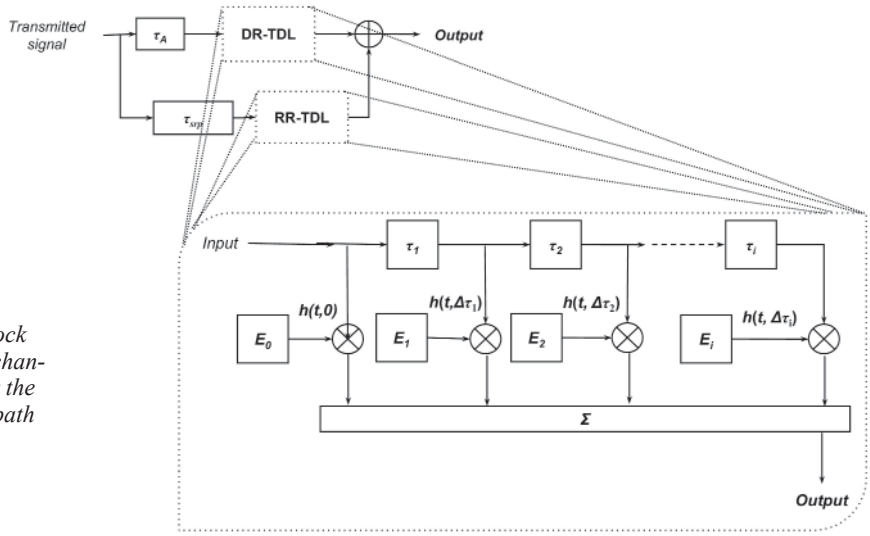


*Figure 6c. A multipath block diagram of the broadband channel modeling simulator for the physical echoes and multipath fading [8, 25, 26].*

$$P_{building} = P\left(h_{mbh} > h_{threshold}\right)$$

$$= \int_{h_{building}}^{\infty} p_{building}\left(h_{mbh}\right) dh_{mbh} \,. \qquad (32)$$

It was then necessary to seek a suitable form for $p_{building}\left(h_{mbh}\right)$ fitting a Rayleigh distribution with the parameter $\sigma_{building}$. The fit was acceptable, although the Rayleigh distribution tended to overemphasize the effects of the building's height. The Rayleigh distribution has the particular advantage in our scheme of being of analytic simplicity. Besides, in the cases where an explicit distribution for the building height was unavailable, the parameter $\sigma_{building}$ can be related to a qualitative classification of the environmental situation. Afterwards, $P_{building}$ is

$$P_{building} = \int_{h_{mbh}}^{\infty} \frac{h_{mbh}}{\sigma_{building}^2} e^{\left(-h_{mbh}/2\sigma_{building}^2\right)} dh_{mbh} \qquad (33)$$

$$= e^{\left(-h_{threshold}^2/2\sigma_{building}^2\right)} .$$

The simplest definition of $h_{threshold}$ was obtained by considering the geometrical block to be represented by the building's face, i.e., $h_{threshould} = h_{LOS}$, which was defined as the height of the direct ray above the building's face relative to the local ground level. In a more-sophisticated approach, the shadowing was considered to occur whenever a significant proportion (say 0.7) of the first Fresnel zone radius, $R_{FZ,LOS}$, of the direct ray was obscured by the building. This case was not considered for the specular reflected ray version. Given that the distance between the HAPS and the building was much greater than the building-to-terminal distance, $R_{FZ,LOS}$ was given by

$$R_{FZ,LOS} = \sqrt{\frac{\lambda x_{TB1}}{\sin\phi\cos\alpha}} \,. \qquad (34)$$

$h_{threshold}$ was thus obtained as

$$h_{threshold} = h_{LOS} - 0.7R_{FZ,LOS} \,. \qquad (35)$$

Subsequently, the functional approaches adopted for the shadowing and line-of-sight cases can be described as

$$f_{CS}(r)|_{shadowing} = p_{vis}(\alpha,\phi) P_{building} f_{shadowing}(r) \,,$$

$$f_{CS}(r)|_{LOS} = p_{vis}(\alpha,\phi) f_{LOS}(r) \qquad (36)$$

Furthermore, other remaining fading factors have been missed in the HAPS literature. The considerations for these significant impairments were reached as following.

In a certain manner, the multipath has a dependence on the carrier wavelength, $\lambda$. For our concise situation, the front-edge wave was contemplated as a reflection from an obstacle or object, if this was smooth and its dimension was large enough compared to $\lambda$. In other words, a smooth facade with large proportions compared to $\lambda$ tends to be a specular reflector, which acts in a manner similar to a mirror. On the other hand, isolated objects with minor size or of size comparable to $\lambda$ cause dispersion of the energy. Consequently, the importance of defining a smooth or rough surface was relevant to the current analysis. The Rayleigh criterion was used, interpreting a height, $h_H$, which should not exceed a critical height of approximately of 2 to 11 cm in our case, as a function of the angle of incidence and $\lambda$.

Accordingly, assumptions for the exterior surfaces of the buildings along the street were made. The majority were taken to consist of brick, stone, or concrete, with many glass windows. These types of surfaces have a poor reflection coefficient at normal incidence, primarily due to the surface roughness and irregularities that are sizeable relative to the RF wavelength. However, at grazing incidence, the surface appears smooth, and its reflection coefficient

becomes highest. The Rayleigh criterion, $h_H \le \lambda/8\cos(\xi)$, determined if a surface was considered smooth, with $\xi$ being the angle of incidence, and $h_H$ being the height of the surface irregularity. In our analysis, $\xi = 8°$ (or greater) was a realistic angle.

In addition to this last consideration, the roughness effects also had an influence on the coherent and specular paths by means of the Rayleigh factor:

$$\zeta = e\left[-\frac{1}{2}\frac{4\pi\sigma_H \cos(\xi)}{\lambda}\right], \qquad (37)$$

where $\sigma_H$ is the standard deviation of the surface roughness. A major weakness in the reflection power of the specular path was deduced with such a factor.

We defined right away that signals traveled at a finite speed. Therefore, an upper limit was defined by the speed of light at the receiver sensing a time delay, $\Delta t$, related to the propagation speed and the distance, $d$: $\Delta t = d/c$. This was chiefly evidenced in the specular reflection path term used. This was also conditioned to the term found for the horizontal distance, $\Delta r_{srp}$, a distance from the "reflection body" to the receiver, and $\alpha$. Ergo, the physical space delay of the reflection path (as shown in Figure 4) was determined by

$$\Delta\tau_{srp} = \tau_B - \tau_A$$

$$= \frac{1}{c}\left(d_{srp} - d_{HAPS}\right) \qquad (38)$$

$$= \frac{1}{c}\left\{\left[\sqrt{\left(\Delta r_{srp} + R_{HAPS}\right)^2 + r_{HAPS}^2} + \left|\Delta r_{srp}\right|\right] - \left[d_{HAPS}\right]\right\}.$$

We have that $\Delta r_{srp} < R_{HAPS}$; $c$ is the speed of light; $d_{srp}$ is the distance from HAPS to the "reflection body" for the specular reflection path; and $\tau_A$ and $\tau_B$ are the arrival delays from HAPS to the terminal for the direct and specular paths, respectively.

The possible attenuation for such a specular reflection path was evaluated from

$$L_{srp,FSL} = 10\log_{10}\left(\frac{d_{srp}}{d_{HAPS}}\right) \text{ [dB]}. \qquad (39)$$

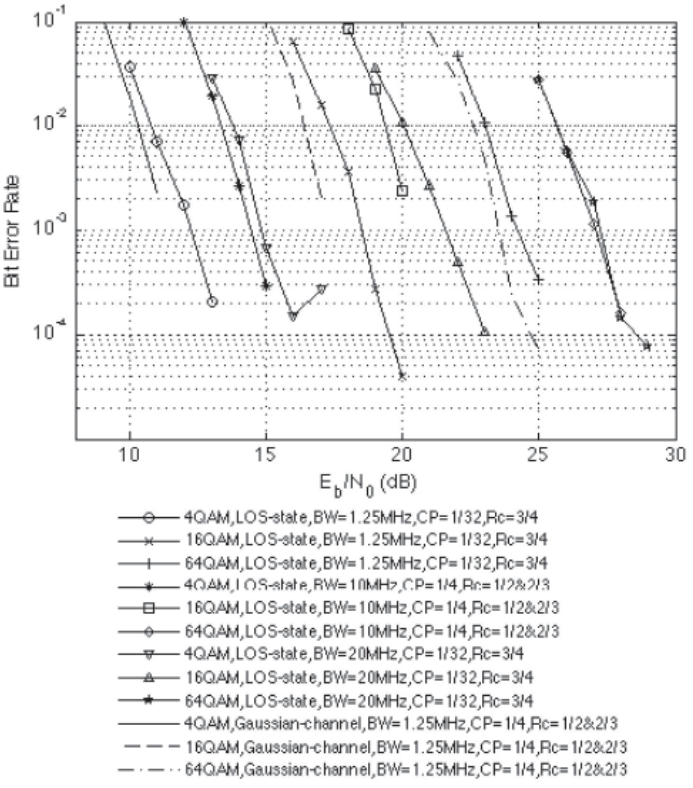


*Figure 7a. As a result of intensive simulations, the WiMAX HAPS-based downlink performance evaluation approach (based on the so-called stratospheric state-oriented channel modeling) is shown for the building-shadowed path. Analyses comprise the geometrical and statistical channel propagation characteristics plus the standardization application by means of the IEEE Std 802.16 WirelessMAN-OFDM air-interface (Fixed-WiMAX).*

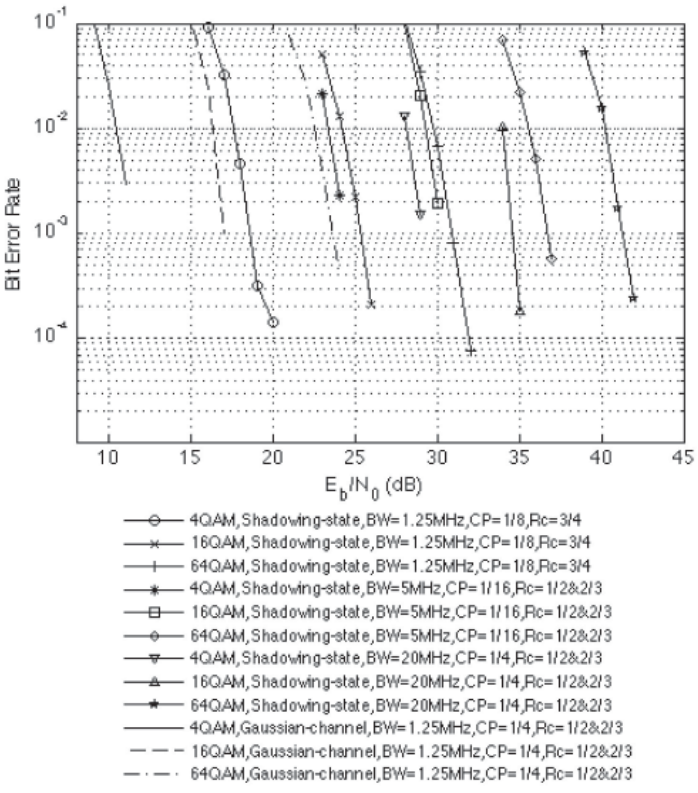


*Figure 7b. As a result of intensive simulations, the WiMAX HAPS-based downlink performance evaluation approach (based on the so-called stratospheric state-oriented channel modeling) is shown for the built-up environment direct path. Analyses comprise the geometrical and statistical channel propagation characteristics plus the standardization application by means of the IEEE Std 802.16 WirelessMAN-OFDM air-interface (Fixed-WiMAX).*

## 4. Performance Results and Discussion

The HAPS-based model was analyzed by means of intensive *MATLAB*-based simulations [31] in the frequency band of 1.820 GHz, following the considerations of IEEE Std 802.16-2004 for the IMT-2000 agenda. We considered a realistic situation, where HAPS provides broadband communications as a fixed wireless-access alternative for the standardization regime. The performance achieved results were qualitatively reasonable, as illustrated in Figure 7 for the specific HAPS-to-terminal elevation angle of 43º (almost at the edge of the defined circular urban-zone coverage of 30º), plus all possible parameters established in the preceding sections. Tables 1 and 2 set for the remaining parameters for usage at the transceiver and the channel-propagation approach. Hence, the results illustrated the outcome for the overall software-aided proposal founded on our analysis hypotheses. Projections of the performance variations under different conditions of modulation (4QAM, 16QAM, 64QAM), coding (Reed-Solomon convolutional coder), and channel characteristics are displayed by means of the bit-error rate (BER) as a function of $E_b/N_{0.}$

The transceiver components (as displayed in Figure 6) were designed around the principles of COFDM. Together with the IEEE standards, this technique supported us with a wide range of operating bandwidths to flexibly address the need for various spectrum-allocation and application requirements, as the alternative outcomes in [25, 26] have already clarified this situation. A brief description of the transmitter block is given, conforming to the main tasks.

*Channel coding:* The channel-coding stage includes randomization, coding, and puncturing. The input data was randomized in order to avoid long runs of ones and zeros. The output of the data randomizer was encoded with a block of a Reed-Solomon-convolutional coder (RS-CC). The convolutional coder constraint length was seven, and its native code rate was one-half. The puncturing block punctured the output of the concatenated encoder to produce variable higher code rates.

*Interleaving:* This block mapped adjacent encoded bits into separated subcarriers, thus minimizing the impact of burst errors caused by spectral nulls.

Modulation: The modulation block converted the sequence of interleaved bits into the sequence of complex symbols, depending on the chosen M-QAM modulation scheme (BPSK, QAM, 16QAM, and 64QAM).

*Data mapping:* The data were introduced to mapping into blocks/frames.

*Pilot insertion:* Pilots were inserted at this point. In addition, at this stage all data symbols were mapped to the data region and their corresponding logical subcarriers.

*IFFT:* The final stage converted the data into the time domain for use at the radio front end, and a guard interval (GI) was inserted after this step.

Table 1 gives the relevant parameters utilized in the transceiver under the standards. The last tasks were applied essentially in order to have a robust and power-spectral-efficient communication outcome, aiming to the alternative of adaptive coding modulation (ACM).

The transceiver parameters were modified into the diverse current system characteristics according to the propagation-channel conditions. Once the time-varying stratospheric channel was estimated, the transmitter was adapted to the new conditions by varying the coding-modulation type, conditioned to maintain a constant error rate. The values of *M*-QAM and RS-CC coding were

| Parameter | Value |
|---|---|
| FFT size | 256 |
| Channel bandwidth, $BW$ [MHz] | 5, 10, 20 |
| Sampling frequency, $F_s$ [MHz] = $nBW$ 8000/8000 ; $n = 8/7$(5 MHz)<br>at licensed band, $n = 57/50$ (10 & 20 MHz) at licensed band | 5.71 (5 MHz),<br>11.4, 22.8 (10 MHz, 20 MHz) |
| Sampling period, $1/F_s$ [µs] | 0.175, 0.087, 0.043 |
| Subcarrier frequency spacing, $\Delta f = F_s/N_{FFT}$ [kHz] | 22.31, 44.5, 89.03 |
| Useful symbol period, $T_b = 1/\Delta f$ [µs] | 44.81, 22.47, 11.23 |
| Guard time, $T_g = T_b CP$ [µs];<br>$CP = 1/4$ and $CP = 1/32$ (cyclic prefix ratio) | 11.2, 5.61, 2.8;<br>1.4, 0.07, 0.035 |
| OFDM symbol duration, $T_s = T_b + T_g$ [µs];<br>$CP = 1/4$ and $CP = 1/32$ (cyclic prefix ratio) | 56.01, 28.08, 14.03;<br>46.21, 22.54, 11.265 |
| No. of used subcarriers | 200 |
| No. of pilot subcarriers | 8 |
| No. of data subcarriers | 192 |
| No. of null subcarriers, and dc subcarriers | 55, 1 |

*Table 1. The parameters in downlink mode for the PHY-layer, IEEE 802.16-2004 [9, 26]*

manually varied. However, they were theoretically related to a switching process, depending on the estimation process controlled by the value of the predicted signal-to-noise ratio. Furthermore, we selected the same modulation case scheme in the way that was applied to all subcarriers. Different modulation was not considered for any group of subcarriers (as possibly carried out by OFDM access, OFDMA).

Two scenes were assumed, according to the surrounding situation at the outdoor terrestrial receiver (as is shown in Figure 5). We contemplated the digital signal scheme consisting of the two main direct and specular reflected rays, which determined the respective fading effect for the short-term set. The objective of this was to quantify the needs of a more-complex channel model, considering real situations that account for the environment and broadband channel characterization. The settled behavior of the whole system clearly developed and differentiated the explicit state-oriented model, where a direct path (Loo's representation) and a shadowing path (Lutz's representation) arose, with the option to be compared to that obtained for the Gaussian case.

| **Parameter** | | |
|---|---|---|
| $f_c$ = 1820 MHz,<br>$\lambda$ = 0.1647 m | $r_{HAPS}$ = 21 km,<br>$R_{HAPS}$ = 0-36.15 km<br>(urban area, $\alpha$ = 90º-30º);<br>$d_{HAPS}$ = 30.72 km,<br>$d_{srp,LOS}$ = 66.14 km,<br>$d_{srp,shadowing}$ = 66.11 km | $\alpha$ = 43º;<br>$R_{HAPS}$ = 22.43 km<br>$\varnothing_{LOS} \leq 10º$,<br>$\varnothing_{shadowing} > 75º$,<br>$\xi$ = 47º |
| $h_{mbh}$ = 20 m,<br>$h_{terminal}$ = 1.5 m,<br>$x_{TB1}$ = 5 m,<br>$x_{BB}$ = 25 m = $x_{building}$,<br>$h_{building}$ = 18.5 m,<br>$\Delta r_{srp,LOS} \leq$ 30 m,<br>$\Delta r_{srp,shadowing} \leq$ 15 m | $L_{LOS}$ = 131.48 dB:<br>$PL_{HAPS,FSL}$ = 127.4 dB,<br>$PL_{Terrestrial,RSL}$ = 0 dB<br>($N_{RB}$ = 0),<br>$PL_{EPLMRB}$ = 0 dB,<br>$PL_{Terrestrial,DD}$ = 4.08 dB;<br>$L_{srp,FSL}$ = 0.0073 dB | $L_{shadowing}$ = 198.91 dB:<br>$PL_{HAPS,FSL}$ = 127.4 dB,<br>$PL_{Terrestrial,RSL}$ = 8.43 dB<br>($N_{RB}$ = 1),<br>$PL_{EPLMRB}$ = 10 dB,<br>$PL_{Terrestrial,DS}$ = 53.08 dB,<br>$L_{srp,FSL}$ = 0.0048 dB |
| $A_{tss}$ = 54%,<br>Shadowing time percentage | $K$ = 5.5 dB<br>Rice-factor | $\mu$ = –13.6 dB ,<br>Mean power relative to LOS under shadowing condition |
| $\sigma$ = 2.9 dB,<br>Standard deviation of lognormal fading | $\tau_A$ = 102.5 µs,<br>$\tau_{B.LOS}$ = 102.67 µs,<br>$\tau_{B,shadowing}$ = 102.58 µs,<br>$\Delta\tau_{srp,LOS}$ = 0.17 µs,<br>$\Delta\tau_{srp,shadowing}$ = 0.097 µs | $N_{echoes,ne} > 50$,<br>$N_{echoes,fe} > 50$<br>No. of multipath echoes at receiver for the diffuse component |
| $i$ = 11 taps (WSSUS tapped-delay-line representation):<br>6 taps at near-echoes, and 5 taps at far-echoes | $\tau_{echoes,ne}$ = [0 0.6) µs,<br>$\tau_{echoes,fe}$ = [0.6-1.2) µs<br>Time duration of near- and far-echoes | $\Delta\tau_i$ = 0.1 µs<br>Equally spaced tap delay |
| Average power of *i-th* tap [$\mu s$]:<br>$MP_{1,ne}$=–24.49, $MP_{2,ne}$=–31.67,<br>$MP_{3,ne}$=–39.21, $MP_{4,ne}$=–49.03,<br>$MP_{5,ne}$=–59.40, $MP_{6,ne}$=–50.40,<br>$MP_{7,fe}$=–51.66, $MP_{8,fe}$=–57.71,<br>$MP_{9,fe}$=–63.49, $MP_{10,fe}$=–69.11,<br>$MP_{11,fe}$=–73.47. | $A_1$ = 0 dB<br>(level power of the direct-signal),<br>$MP$ = –23.6 dB | $A_2$ = –10 dB<br>(level power of the specular reflection signal),<br>$MP$ = –26.8 dB |
| $S_{p,ne}$ = 10 dB/µs,<br>$S_{p,fe}$ = 10 dB/µs<br>Multipath power slope decay | $\tau_{e,ne}$ = 0.069 µs,<br>$\tau_{e,fe}$ = 0.091 µs<br>Average distribution for excess delay (near- and far-echoes) | $\tau_{m,ne}$ = 0.6 µs,<br>$\tau_{m,fe}$ = 1.2 µs<br>Maximum excess delay (near- and far-echoes) |
| $f_{D,max}$ of ~2.4 Hz,<br>Maximum Doppler shift | $T_{coherence} \approx 1/f_{D,max}$ = 0.416 s,<br>Coherence time | $BW_{coherence} \approx 1/\tau_m$ = 833.33 kHz,<br>Coherence bandwidth |

*Table 2. Radio propagation and channel-fading characteristics.*

The analysis processes given in the previous sections have provided a practical means of incorporating the shadowing case for a built-up area, and the unobstructed-path situation, for an accurate HAPS-based transmission link prediction. Environmental situations have been successfully applied to predict the median field strength and fading over the received signal with good accuracy. We prevented the transmission system from counteracting against the signal attenuation and variations with low computational complexity and simple physical data. We can note that the result might particularly have been a worse outcome for the shadowing case (Figure 7a), which effect should not have had a high impact on the system's performance, in spite of the high elevation-angle value of 43º. However, within the built-up environment influenced by the visibility and building heights, plus a low code rate, low cyclic prefix ratio, and high nominal bandwidth usage, the signal underwent low performance (Figure 7a). The complete calculations also showed that the performance got better for the direct path (Figure 7b), because of the existence of the line-of-sight situation, and less impact from the built-up structures.

Moreover, the owned application and simulation have been virtually required that one can have line of sight state communications much of the time given the power limited nature of the actual surreal HAPS-based system. The concept of the combination of the shadowed and un-shadowed cases (i.e., the state-oriented model) was performed, but without the actions to introduce it into a single-channel simulation run. Rather, it was compared with the two possible scenarios existing within the urban-area coverage. We assumed that the channel was in each of the states for a certain percentage of time (with help from the land-mobile satellite system empirical approaches). Separate simulations were then conducted, using each of the models. The outcomes were then combined in a uniform manner according to the suppositions of the percentage of time spent in each state.

The implementation of this last approach has limitations based on neglecting the channel state's transition effects, where the communication condition would be changing from one state to another. The fading-mitigation techniques may be sensitive to such changes for each case.

Correspondingly, we can remark that singularly, very little measured and other advanced theoretical data exist nowadays to use as references for comparison to our model, specifically with the specifications used for performance evaluation. Hence, worth limitations for our HAPS-based proposal where presumed in order to reflect the real application as a wireless access system. However, on the positive side for the broadband application, we had an approximation to the fading countermeasures with the technology used. These can possibly be compared with the general and real performance predictions from wireless terrestrial studies; shadowing and direct conditions could be included.

The system demonstrated in this case is an ongoing work. Based on simulations, it has been proven that the HAPS-based approach model can be an alternative and supportive system to those wireless systems already defined for practical real applications, based on data primarily obtained from terrestrial and satellite campaign research. In the interim, the utilization of channel coding and OFDM techniques were sufficient requirements to realize palpable, reliable, and robust communications based on a stratospheric platform for the metropolitan coverage service area.

## 5. Conclusions

This paper has presented a WiMAX HAPS-based downlink performance analysis, using a proposal for the HAPS-to-fixed terminal channel at L band. Free-space loss plus deterministic ray tracing and statistical approaches have been used to provide more realistic predictions of the HAPS service coverage sector for a stipulated building grouping and position. Miscellaneous simulations by means of bit-error rate as a function of $E_b/N_o$ were achieved for the performance of the system, using the air-interface scheme proposed in fixed WiMAX. The COFDM technique offered advantages for our specific conditions of channel modeling and environment. Finally, it was observed that additional work is also needed to determine methods to open the fixed condition to mobility of both the receiver and the platform.

## 6. Acknowledgements

The authors would like to thank the anonymous reviewers for their helpful comments and suggestions, which have significantly improved this paper. This work was partially supported by the EU under IST Project Capanina (FP6 IST-2003-506745) and the Spanish Government Project TEC2004-0136-E. The authors were members of COST297-High Altitude Platforms for Communications and Other Services (HAPCOS) (European Action ending by 2009). Thanks to the CONACyT Program (National Financial Resource in Mexico for Science and Technology) for corresponding to the financial support.

## 7. References

1. G. M. Djuknic and Y. Okunev, "Establishing Wireless Communications Services via High-Altitude Aeronautical Platforms – A Concept Whose Time Has Come?," *IEEE Communications Magazine*, **35**, 9, 1997, pp. 128-35.
2. Y. Hase, R. Miura, and S. Ohmori, "A Novel Broadband All-Wireless Access Network Using Stratospheric Platforms," The 48th IEEE Semi-annual Vehicular Technology Conference (VTC-1998 Spring), 2, 1998, pp. 1191-94.
3. T. C. Tozer and D. Grace, "High-Altitude Platforms for Wireless Communications," *Electronics & Communication Engineering Journal*, **13**, 3, 2001, pp. 127-37.
4. A. K. Widiawan and R. Tafazolli, "High Altitude Platform Station (HAPS): A Review of New Infrastructure Development for Future Wireless Communications," *Wireless Personal Communications*, **42**, 3, 2007, pp. 387-404.

5. Stylianos Karapantazis and Fotini-Niovi Pavlidou, "Broadband Communications via High-Altitude Platforms: A Survey," *IEEE Communications Surveys & Tutorials*, **7**, 1, 2005, pp. 2-31.

6. International Telecommunication Union, Radiocommunications Sector, "Minimum Performance Characteristics and Operational Conditions for High Altitude Platform Stations Providing IMT-2000 in the Bands 1885-1980 MHz, 2010-2025 MHz, and 2110-2170 MHz in the Regions 1 & 3, and 1885-1980 MHz and 2110-2160 MHz in Region 2," ITU-R M.1456, 2000.

7. M. A. Vázquez-Castro, D. Belay-Zeleke, and A. Curieses-Guerrero, "Availability of Systems Based on Satellites with Spatial Diversity and HAPS," *IEE Electronics Letters*, **38**, 6, 2002, pp. 286-88.

8. María Vázquez-Castro and Fernando Pérez-Fontán, "Channel Modeling for Satellite and HAPS System Design," *Wireless Communications and Mobile computing*, **2**, 3, 2002, pp. 285-300.

9. IEEE, "802.16™ – IEEE Standard for Local and Metropolitan Area Networks, Part 16: Air Interface for Broadband Wireless Access Systems," IEEE Std 802.16™-2009 (Revision of IEEE Std 802.16-2004).

10. International Telecommunication Union, Radiocommunication Sector, "Detailed Specifications of the Radio Interfaces of International Mobile Telecommunications – 2000 (IMT-2000)," ITU-R M.1457, 2001-2007.

11. S. Karapantazis and F. N. Pavlidou, "Broadband from Heaven [High Altitude Platforms]," *IEE Communications Engineer*, 2004, pp. 18-24.

12. A. Aragón-Zavala, Cuevas-Ruíz, and J. A. Delgado-Penín, *High-Altitude Platform Systems for Wireless Communications*, New York, John Wiley & Sons, 2008, p. 256.

13. M. Iskandar and Shigueru Shimamoto, "On the Performance of IMT-2000 Communication Link based on Stratospheric Platforms," *Makara, Teknologi (Fakultas Teknik Universitas Indonesia)*, **10,** 1, 2006, pp. 1-10.

14. Marina Mondin, Favio Dovis, and P. Mulassano, "On the Use of HALE Platforms as GSM Base Stations," *IEEE Personal Communications*, **8**, 2, 2001, pp. 37-44.

15. F. Davarian, "Channel Simulation to Facilitate Mobile-Satellite Communications Research," *IEEE Transactions on Communications*, **35**, 1, 1987, pp. 47-56.

16. A. Jahn, "Propagation Data and Channel Model for LMS Systems," European Space Agency Final Report (DLR German Aerospace Research Establishment Institute for Communications Technology, Institut Für Nachrichtentechnik), 1994.

17. M. A. N. Parks, S. R. Saunders, and B. G. Evans, "A Wideband Channel Model Applicable to Mobile Satellite Systems at L- and S-Band," IEE Colloquium on Propagation Aspects of Future Mobile Systems, Digest No. 1996/220 (12), 1996, pp. 1-6.

18. Riu Miura and Mikio Suzuki, "Preliminary Flight Test Program on Telecom and Broadcasting Using High Altitude Platform Stations," *Wireless Personal Communications*, **24**, 2, 2003, pp. 341-61.

19. Matthias Pätzold, *Mobile Fading Channels*, New York, John Wiley & Sons, 2002.

20. S. R. Saunders and F. R. Bonar, "Prediction of Mobile Radio Wave Propagation Over Buildings of Irregular Heights and Spacings," *IEEE Transactions on Antennas and Propagation*, **AP-42**, 2, 1994, pp. 137-44.

21. S. R. Saunders and B. G. Evans, "A Physical-Statistical Model for Land Mobile Satellite Propagation in Built-Up Areas," 10th International Conference on Antennas and Propagation (IEE), 1997, pp. 44-47.

22. D. M. Le Vine and M. A. Karam, "Dependence of Attenuation in a Vegetation Canopy on Frequency and Plant Water Content," *IEEE Transactions on Geoscience Remote Sensing*, **34**, 1996, pp. 1090-96.

23. A. Czylwik, "OFDM and Related Methods for Broadband Mobile Radio Channels," Proceedings of International Zürich Seminar on Broadband Communications. Accessing, Transmission, Networking, Zürich, Switzerland, 1998, pp. 91-98.

24. E. Falletti, M. Laddomada, M. Mondin, and F. Sellone, "Integrated Services from High-Altitude Platforms: A Flexible Communication System," *IEEE Communications Magazine*, **44**, 2, 2006, pp. 85-94.

25. I. R. Palma-Lazgare, J. A. Delgado-Penin, and F. Perez-Fontan, "An Advance in Wireless Broadband Communications Based on a WiMAX-HAPS Architecture," 26th International Communications Satellite Systems Conference (ICSSC'2008), San Diego, CA, 2008.

26. I. R. Palma-Lazgare and J. A. Delgado-Penin, "Fixed Broadband Wireless Access Based on HAPS Using COFDM Schemes: Channel Modelling and Performance Evaluation," Australasian Telecommunication Networks and Applications Conference (ATNAC 2008), Adelaide, SA, Australia, pp. 62-66.

27. Erich Lutz, D. Cygan, M. Dippold, and W. Panke, "The Land Mobile Satellite Communication Channel –Recording, Statistics, and Channel Model," *IEEE Transactions on Vehicular Technology*, **40**, 2, 1991, pp. 375-93.

28. C. Loo and J. S. Butterworth, "Land Mobile Satellite Channel, Measurements and Modeling," *Proceedings of the IEE*, **86**, 7, 1998, pp. 1442-63.

29. P. A. Bello, "Characterization of Randomly Time-Variant Linear Channels," *IEEE Transactions on Communications Systems*, **11**, 4, 1993, pp. 360-93.

30. M. Iskandar and Shigeru Shimamoto, "On the Downlink Performance of Stratospheric Platform Mobile Communications Channel," The 49th Annual IEEE GLOBECOM, San Francisco, CA, 2006.

31. Fernando Pérez Fontán and P. Mariño Espiñeira, *Modeling the Wireless Propagation Channel, A Simulation Approach with Matlab®*, 2008.